Chapter

Numerical Analysis of a Water-Cooled Condenser at Startup Conditions for Refrigeration Applications Supported with Experiments

Carlos Acosta

Abstract

Refrigeration for commercial purposes is one of the industrial sectors with the largest energy consumption in the global market. Therefore, research and development of more efficient components such as compressors, condensers, and refrigerants continue to render promising results in terms of GWP and operational costs. However, Due to the urgency typically found in industry to develop prototypes, finding scalable solutions can be challenging. Arguably, this is the case for condenser and evaporators that are designed and assembled under the assumption that refrigeration systems operate at steady condition, where in real circumstances such systems operate under transients based on ambient temperatures or unfavorable startup conditions. The aim of this study is to characterize the thermal and fluid dynamics behavior of refrigerant R404a in a water-cooled condenser at startup conditions. The boundary conditions to solve the CFD simulations are taken from experimental values and set as user defined functions in a commercial software. The results displayed the time dependent oscillatory phase-transition details of the refrigerant throughout the domain.

Keywords: Heat transfer, fluid mechanics, multi-phase flow, turbulence, phase-transition

1. Introduction

Water-cooled condensers are commonly used in vapor compression refrigeration for industrial applications due to their high rate of heat transfer [1], simple configuration and the relatively low cost of manufacturability compared to other types of condensers [2]. On the other hand, population growth, and the exponential increase in energy consumption throughout the world keep stressing freshwater resources [3]. Typical components used in refrigeration systems such as compressors, evaporators, condensers, and refrigerants are constantly iterating to provide more energy efficient solutions [4] in order to minimize the environmental impact due to toxic molecules in refrigerants and reduce the production of residual heat [5]. Unfortunately, the steps imposed by regulatory agencies in United States and

Europe sometimes lead to production ready solutions that have not been thoroughly tested for industrial applications. Perhaps, one common example is the race in banning HFC refrigerants for compressed vapor refrigeration cycles [6]. Ideally, the components in the refrigeration system can remain intact by changing refrigerants, but this fails to be the case for most systems since the oil in the compressor and even the compressor specifications need to be tailored to the new refrigerant [7].

Virtual experimentation using numerical simulations offer great insights at the micro and macroscopic level to support design and research activities of heat exchangers, condensers and evaporators [8] given that experimental studies can reach elevated costs and access to sensorial points to capture significant physical details are difficult to incorporate in pressurized systems [9, 10]. In fact, the analysis of startup condition for physical components in thermodynamic cycles is particularly challenging given the small-time scales and the large variations detected in the variables of interest [11]. This alone calls for special attention in the sampling rate and physical location of feedback sensors given that dynamic and unstable conditions can be reached in a thermodynamic cycle by unpredicted changes in loads or variations in energetic states, and false positive readings can be measured depending on the flow characteristics through the system.

Concomitantly, the design and fabrication of condensers and heat exchangers require the knowledge and understanding of the physical and chemical phenomenon and other factors such as the properties of the working fluids or multi-phase flows [12], their regimes and states, and the geometrical characteristics of the system [13]. But rigorous experimentation in thermodynamic systems can be particularly costly because environmental chambers are often needed to obtain reproducible results [14]. Evidently, the lack of accessibility to an environmental chamber means that the ambient temperature is a random variable and the uncertainty of the experimental results can increase significantly [15] since the thermodynamic states of the thermodynamic cycle tend to fluctuate as a function of the heat rejected and the heat absorbed to and from the environment [16].

A less rigorous alternative to this approach is to perform a design of experiments at ambient conditions and execute the test multiple times to assess the error and response variations [17]. Unfortunately, this route can also lead to an expensive and time-consuming solution on top of developing variable startup conditions that can affect the performance of the system. Consequently, Numerical simulations and theoretical analysis of thermodynamic cycles should help alleviate the cost of materials, manufacturing, and redundant testing.

Heat and time-dependent multi-phase computational solutions targeting problems with complicated geometries that cannot be simplified by axisymmetric conditions or reduction of dimensions tend to be challenging to develop, and the results are always suspicious if no experimental validation is provided. Therefore, a balance between experiments and simulations seems to be the ideal recipe to obtain cost-effective solutions with solid scientific ground.

In the last few decades, significant efforts have been focused on developing more rigorous models that account for turbulent fluctuations on mufti-phase flows [18–20] evidencing the complicated nature of such problems even for simple geometries [21] such as tubes and channels [22]. However, no three-dimensional studies have been reported on the CFD multi-phase modeling of R404a condensation in a medium temperature water-cooled condenser at startup conditions. This research aims to provide a study of the unsteady condensing and evaporating characteristics of R404a in a water-cooled condenser by modeling the raising temperature and pressure in the system induced by the compressed vapor entering the condenser based on experimental data.

1.1 Numerical analysis of turbulent phase-transition in the condensation process of refrigerant flow

Multi-phase flow refers to the flow of a mixture of phases or species such as gases in liquids or liquids in gases of different densities [23] where the liquids, and gases are considered distinct phases. There are different mathematical characterizations targeted to study multi-phase flows. For instance, for dispersed flows, one phase consists of discrete, noncontinuous elements (such as bubbles) and the second phase is considered as a continuum. This approach is widely accepted for the analysis and characterization of oil and refrigerant relationships in vapor compressed cycles, given that at certain conditions, oil can scape the compressor and affect the system performance due to the variations in the thermal properties of the mixture induced by the oil [24].

In bubbly flows or other types of applications where dispersed multiphase flows are applicable, the properties of the inhomogeneous mixture are defined relative to the continuous phase [25]. The mathematical manipulation for such flows can happen under a Lagrangian representation for the dispersed phase [26], and an Eulerian reference for the continuous phase. For the continuous phase, the material properties are defined at every point within a control volume [27], whereas in a separated flow under the Euler–Euler approach the phases are continuous but divided by a single contact surface [28].

This research focuses on the incompressible volume of fluid model where the mass transfer between phases is given by:

$$\dot{m}_v = -\dot{m}_l = \varsigma \alpha_l \rho_l \left[\frac{T - T_{sat}}{T_{sat}}\right], T > T_{sat} \tag{1}$$

for evaporation and

$$\dot{m}_l = -\dot{m}_v = \varsigma \alpha_v \rho_v \left[\frac{T_{sat} - T}{T_{sat}}\right], T < T_{sat} \tag{2}$$

for a condensation process. In the study of phase-transition of refrigerants, the saturation temperature is found based on the operating conditions of the system [29]. In this study, the inlet and outlet temperatures and pressures were measured experimentally to compute T_{sat}.

From a modeling perspective, the saturating temperature is a dominant factor in the prediction of the evaporating and condensing process. Therefore, the measured temperatures, pressures and the saturation temperature were loaded in the simulation as dynamics boundary conditions to drive the phase-transition process given the dynamic value of T_{sat}.

In order to find the quality of the mixture the volume fraction is defined as:

$$\alpha_l(\tilde{X}) + \alpha_v(\tilde{X}) = 1 \tag{3}$$

where the sum of volume occupied by the phases is 100%. Furthermore, the microscopic dynamics of the phase-transition process of refrigerants in heat exchangers and condensers can be studied by considering both the vapor and liquid as continuous and interpenetrating fluids under the Eulerian frame of reference [30]. Even though this approach is computationally expensive given that the governing equations for each phase are solved together with the momentum equation, the mass diffusion can be monitored by a straightforward calculation. For this case, the microscopic behavior of the phases can be monitored by:

$$\frac{\partial \alpha_l}{\partial t} + \nabla \cdot \left(\vec{u}\alpha_l\right) = \frac{\dot{m}_l}{\rho_l} = S_{mass} \tag{4}$$

and

$$\frac{\partial \alpha_v}{\partial t} + \nabla \cdot \left(\vec{u}\alpha_v\right) = -\frac{\dot{m}_v}{\rho_v} = -S_{mass} \tag{5}$$

for which ρ_l and ρ_v are the densities of the liquid and vapor phases. Then. the mixture density and mixture viscosity are:

$$\rho_m = \rho_l + \rho_v \tag{6}$$

and

$$\mu_{\mathrm{m}} = \mu_l + \mu_v. \tag{7}$$

For each phase, the momentum conservation is given by:

$$\frac{\partial}{\partial t}\left(\alpha_v \rho_v \vec{u}_v\right) + \nabla \bullet \left(\alpha_v \rho_v \vec{u}_v \bullet \vec{u}_v\right) = -\alpha_v \nabla \mathrm{p} + \nabla \bullet \bar{\bar{\tau}}_v + \psi_v \tag{8}$$

and

$$\frac{\partial}{\partial t}\left(\alpha_l \rho_l \vec{u}_l\right) + \nabla \bullet \left(\alpha_l \rho_l \vec{u}_l \bullet \vec{u}_l\right) = -\alpha_l \nabla \mathrm{p} + \nabla \bullet \bar{\bar{\tau}}_l + \psi_l \tag{9}$$

where ψ_v and ψ_l are the momentum sources and the stress tensor is given by:

$$\bar{\bar{\tau}}_i = \alpha_i \mu_i \left(\nabla \vec{u}_i + \nabla \vec{u}_i^{\,T}\right) + \alpha_i \left(\lambda_i - \frac{3}{2}\mu_i\right) \nabla \bullet \vec{u}_i \, \bar{\bar{I}} \tag{10}$$

given that λ_i and μ_i are the shear and bulk viscosities of the phase i. Then, the two equation $\kappa - \varepsilon$ turbulent model for multi-phase flow is:

$$\frac{\partial}{\partial t}\left(\alpha_v \rho_v \kappa\right) + \nabla \bullet \left(\alpha_v \rho_v \kappa \vec{u}_v\right) = \frac{\partial}{\partial x_j}\left[\alpha_v \left(\mu + \frac{\mu_t}{\sigma_\varepsilon}\right)\frac{\partial \kappa}{\partial x_j}\right] - \alpha_v \rho_v \varepsilon + \alpha_v G_k + S_k \tag{11}$$

for the turbulent kinetic energy κ and

$$\frac{\partial}{\partial t}\left(\alpha_v \rho_v \varepsilon\right) + \nabla \bullet \left(\alpha_v \rho_v \varepsilon \vec{u}_v\right) = \frac{\partial}{\partial x_j}\left[\alpha_v \left(\mu + \frac{\mu_t}{\sigma_k}\right)\frac{\partial \varepsilon}{\partial x_j}\right] - \alpha_v \mathrm{C}_{1\varepsilon}\frac{\varepsilon}{\kappa}G_k - \alpha_v C_{2\varepsilon}\rho_v \frac{\varepsilon^2}{\kappa}G_k + S_\varepsilon \tag{12}$$

for turbulent dissipation ε where $\mu_t = C_\mu \rho_v \frac{\kappa^2}{\varepsilon}$ and $C_\mu = 0.99$.

The thermal energy in the process is conserved and computed for each phase by:

$$\frac{\partial}{\partial t}\sum_i \left(\alpha_i \vec{u}_i (\rho_i E_i + P)\right) = \nabla \bullet \left(K_f \nabla T\right) \tag{13}$$

Where the energy is $E = h_i - \frac{P}{\rho_i} + \frac{\vec{u}_i^{\,2}}{2}$ and the enthalpy and effective thermal conductivity are:

$$h = \frac{\alpha_l \rho_l h_l + \alpha_v \rho_v h_v}{\alpha_l \rho_l + \alpha_v \rho_v} \tag{14}$$

$$h_l = C_{p,l}(T - T_o), h_l = C_{p,v}(T - T_o), \tag{15}$$

$$K_{eff} = \alpha_l K_l + \alpha_v K_v. \tag{16}$$

2. Experimental procedure

Since the energetic state of a refrigerant far from its critical point can only exist for stable conditions at a single pressure and temperature pair [31], it is crucial to properly identify the coupled operating pressures and temperatures to obtain the saturated temperature of the refrigerant. For this reason, an experimental setup was designed and constructed so that the inlet and outlet conditions of the water and the refrigerant under transient conditions can be detected and used as dynamic boundary conditions for the numerical simulation.

The water-cooled condenser was fabricated using copper tubing. The dimensions for the line of water, refrigerant line and copper wall separation are shown in **Table 1**. To enhance the heat transfer, thermal insulation (Polyethylene foam) was placed around the water copper jacket and the rest of the tubbing connecting the components in the refrigeration system.

Figure 1 shows the configuration adopted to characterize the condensing details of R404a. The figure shows the standard cycle corresponding to a vapor compression cycle including the compressor (Copeland ZB15-KCE), the water-cooled condenser, the evaporator, and the thermostatic expansion valve (Danfoss T2). The temperature and pressure of the vapor and liquid refrigerant were measured at points (1) and (2) by attaching thermocouples to the refrigeration line and connecting pressure transducers to measure the pressure drop of the refrigerant across the helix. The water inlet and outlet temperatures are monitored (3) and (4) in a non-invasive fashion.

The test methodology consisted of 6 consecutive runs for 4.75 minutes each in order to stabilize the system and reach thermal equilibrium given that an environmental chamber was not used for this study. A flow meter (5) and pressure regulator are located at the water inlet to measure the flow rate and sustain the water pressure.

Table 2 shows the magnitude of the variables monitored to control the steady performance of the system.

Parameter	Dimension
D_{Ω_1}	0.0254 $[m]$
$D_{\Omega_{2-in}}$	0.0127 $[m]$
$D_{\Omega_{2-out}}$	0.0147 $[m]$
D_{Ω_3}	0.0127$[m]$
Pitch	0.031$[m]$
D_{HLX}	0.213 $[m]$
L_{arc}	3.05$[m]$
$A_{s-\Omega_1}$	0.3847 $[m^2]$
$A_{s-\Omega_{2-out}}$	0.2127 $[m^2]$
$A_{s-\Omega_3}$	0.1834$[m^2]$

Table 1.
Parameters and dimension of the water-cooled condenser.

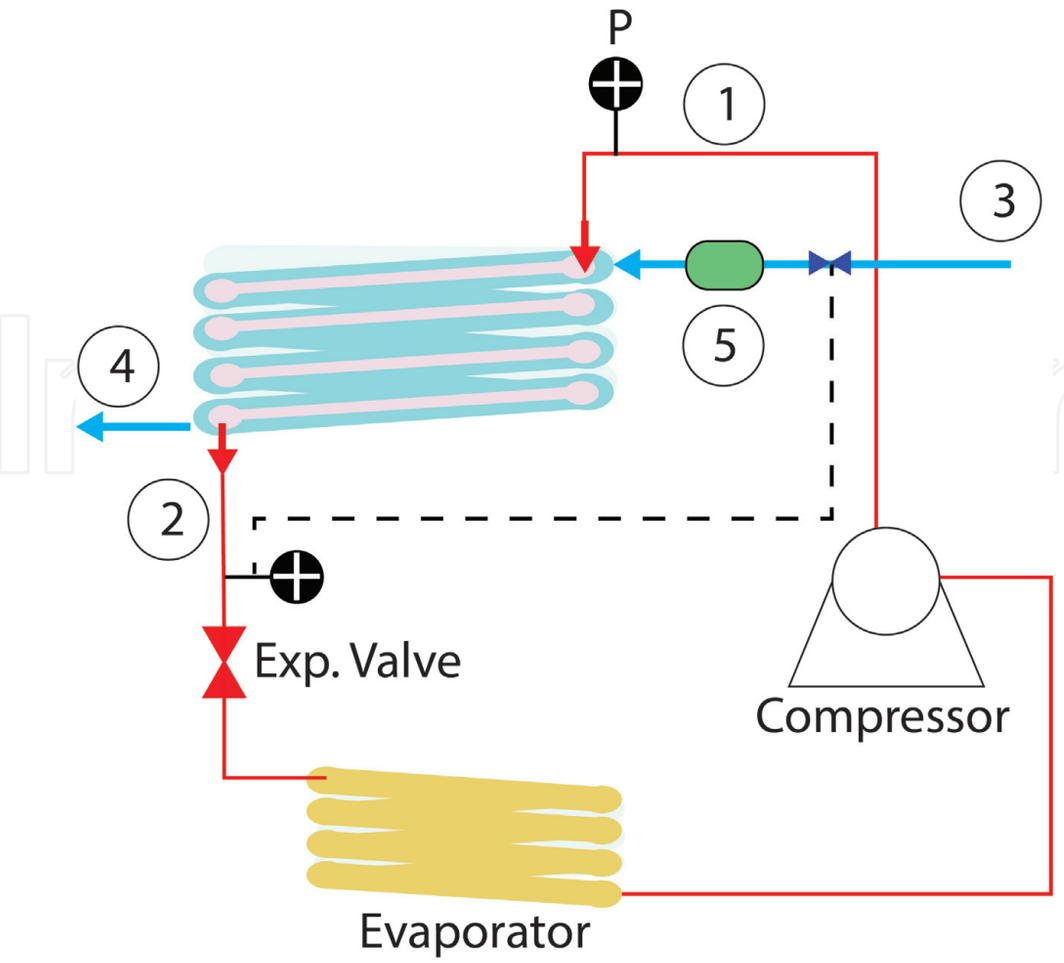

Figure 1.
Schematic representation of the refrigeration system depicting the testing points measuring the inlet and outlet temperature and pressure of the refrigerant at (1) and (2), as well as the water temperature at the inlet and outlet at (3) and (4).

Table 3 shows the sensors and instruments used for the experimental study as well as the accuracy reported by the manufacturers. The sampling rate was fixed to 100 ms using LabView 18 software and the corresponding hardware with the data acquisition system to gather the temperatures and pressures values of both water and refrigerant.

The water and refrigerant temperature at the inlet and outlet of the condenser are reported in **Figure 2** with the corresponding variation to document the test repeatability. The figure also shows the measured refrigerant pressure and the computed liquid saturation temperature using Coolproops 6.4.1 [32].

The experimental data demonstrated that the system reached maximum operating pressure close to 300 ms after starting the compressor, and a steady-state condition

Variable	Magnitude
Super-heat	25 ± 2.5 [°C]
Sub-cool	18 ± 2.5 [°C]
T_∞	22 ± 0.9 [°C]
$\dot{m}_{R404a}$	$0.398 \left[\frac{kg}{s}\right]$

Table 2.
Operational parameters of the refrigeration system.

Variable	Instrument	Accuracy
P	Transducer (PX-309)	0.25%Full Scale
T	J-Type Thermocouple	±2.2°C
$\dot{m}_{H_2O}$	2321FG	2.0%Full Scale

Table 3.
Instrumentation.

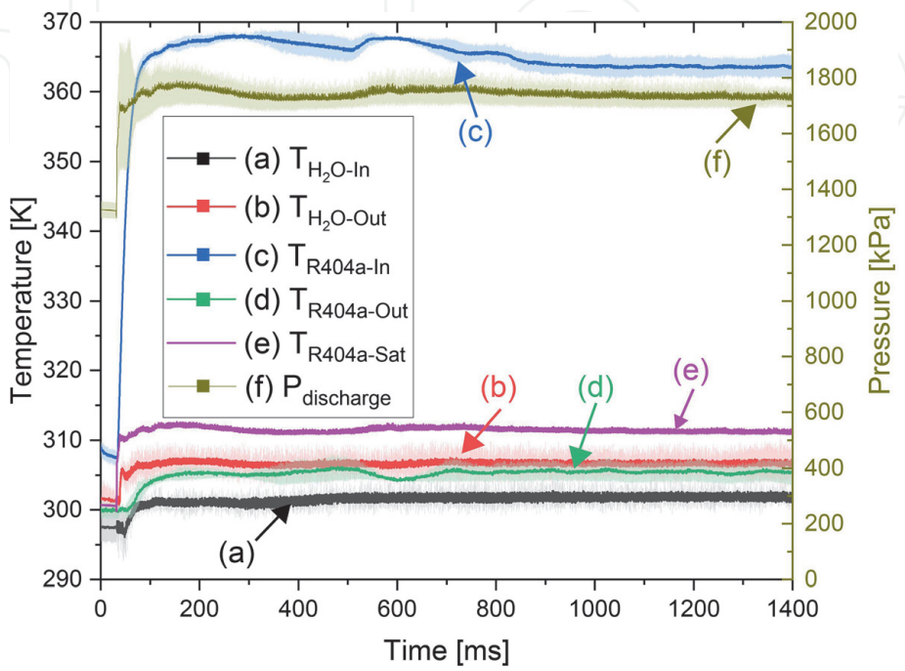

Figure 2.
Experimental data obtained experimentally and computed saturation temperature of R404a.

for the vapor refrigerant pressure was reached around 1200 ms after initialization. In order to characterize the startup conditions, the first 2000 ms of the average between the different experiments corresponding to each variable displayed in the **Figure 2** were programed in ANSYS Fluent as dynamic boundary conditions.

3. Computational domain and boundary conditions

A time-dependent numerical model in three-dimension was developed to simulate the phase-transition and heat transfer of R404a in a water-cooled condenser. The geometry accounts for two fluid regions as well as one solid domain (copper) that separates both flows and provides the thermal mechanism for heat transfer. The computational domain $(\Omega_1 \cup \Omega_2 \cup \Omega_3)$ contains three distant regions belonging to the space $\tilde{X} \rightarrow R^3$ assigned as follows:

a. Fluid region for water (Ω_1).

b. Solid copper region for physical division of water and refrigerant (Ω_2).

c. Fluid region for refrigerant R404a (Ω_3).

The properties of the materials and working fluids are show in **Table 4**. The temperature dependent material properties were programmed in Fluent using

Property	unit	Substance/Material			
		Water	R404a vapor	R404a liquid	Copper
K	$\left[\frac{W}{mK}\right]$	0.6 [33]	0.015 [34]	0.063 [34]	387.6 [35]
ρ	$\left[\frac{kg}{m^3}\right]$	$799.71 + 1.6040\text{T} - 3.161\text{x}10^{-3}T^2$ [33]	65.24 [34]	$\rho_{l-R404a}(T)$ [34]	8978 [35]
c_p	$\left[\frac{J}{kg\ K}\right]$	4182 [36]	1221.4 [37]	1542.3 [34]	381 [35]
μ	$\left[\frac{kg}{m\ s}\right]$	$\frac{997.2}{2.4432\text{x}10^{-2}\text{T}-6.1536}$[38]	$\mu_{v-R404a}(T)$ [36]	$\mu_{l-R404a}(T)$ [36]	
ξ_l	$\left[\frac{mN}{m}\right]$	7.52 [37]			
M	$\left[\frac{g}{mol}\right]$	18.6 [33]	97.6 [37]		
$T_{cr-R404a}$	$[K]$	345.25 [39]			
$T_{o-R404a}$	$[K]$	227.15 [39]			

Table 4.
Physical properties of the water, copper, and refrigerant regions.

transient data tables and user defined routines. A schematic representation of the domains describing the computational domain is shown in **Figure 3**. The figure shows the inlet and outlet faces assigned for the water and refrigerant flows. The 3D geometry was modeled in SpaceClaim from the real dimensions and the numerical solution was obtained using Ansys Fluent 19.2. The contacting surfaces were discretized with conformal elements and the computational grid was created using tetrahedral objects with a maximum Skewness of 0.74. The mesh contains 36040897 nodes and 119573669 elements with a mean size of 3.12e-2[m].

The residual target (RMS) for the momentum and energy equations were set to $1e-3$ and $1e-5$ respectively. The time step was fixed to $1e-6$ for a total simulation time of 2 seconds.

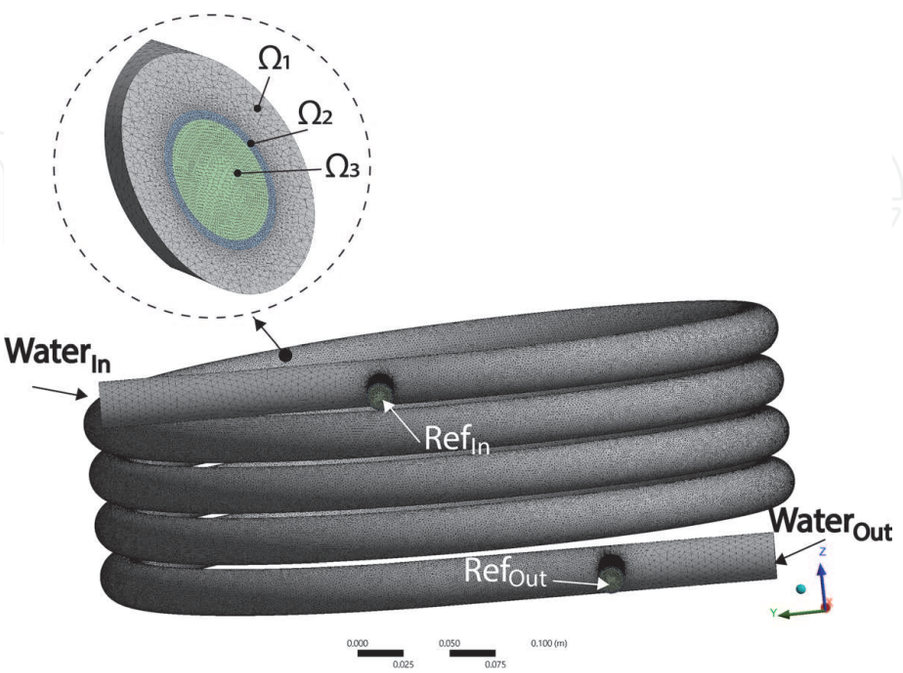

Figure 3.
Three-dimensional computational domain specifying the fluid and solid regions considered for the numerical simulation.

Model validation and verification against experimental data is an important aspect of any numerical solution. For turbulent multi-phase flows, the model validation for the phase-transition process is particularly important because the solution of the volume fraction equation depends on the saturation temperature [40]. However, the model validation and identification of the saturation temperature can be challenging if the geometry is complex enough to obstruct the path of light for particle image velocimetry and particle image thermometry or block the access of probes for electric tomography techniques [41]. Unfortunately, the phase-transition process in the water-cooled condenser complies with the restrictions mentioned above because the refrigerant phase-transition takes place in a region where standard field experimental techniques offer limited information due to the water and copper jacket around the refrigerant line. Therefore, in order to develop a model that resembles reality, the saturation temperature has been programmed as a boundary condition based on the inlet and outlet temperatures and pressures measured experimentally.

3.1 Boundary conditions

The inlet boundary conditions for water and refrigerant are set to the mean mass flows. The flow rate of water measured experimentally going into the system ranges from 0.21 to $0.3\frac{kg}{s}$ and the inlet refrigerant mass flow corresponds to the compressor mass flow provided by the manufacturer at the operating conditions.

The inlet and outlet time dependent temperature, pressures, and saturation temperature are loaded as user functions in Fluent from the experimental values shown in **Figure 2**. A no slip velocity condition was assigned to the boundary walls $\left(\vec{u}_{\partial\Omega_i} = 0\right)$ and a thermal insulation condition was assigned on the wall between the water and the environment. The outlet quality was set to 100% liquid given that the actual system was designed and fabricated with the charge and specifications to hold a constant sub-cool temperature after the condenser.

$\dot{m}_{in-R404a}$	$0.398\left[\frac{kg}{s}\right]$
$P_{G-in-R404a}$	From experiments (see **Figure 2**)
$P_{G-out-R404a}$	From experiments (see **Figure 2**)
$T_{in-R404a}$	From experiments (see **Figure 2**)
$T_{out-R404a}$	From experiments (see **Figure 2**)
$x_{in-R404a}$	0
$x_{out-R404a}$	1
$\dot{m}_{in-H_2O}$	$0.26\left[\frac{kg}{s}\right]$
P_{out-H_2O}	$0[Pa]$
T_{in-H_2O}	From experiments (see **Figure 2**)
T_{out-H_2O}	From experiments (see **Figure 2**)
$\vec{u}_{\partial\Omega_1} = \vec{u}_{\partial\Omega_{2-in}} = \vec{u}_{\partial\Omega_{2-out}} = \vec{u}_{\partial\Omega_3}$	0
$\frac{\partial T_{\partial\Omega_{3-\infty}}}{\partial n}$	0
$-Q_{\partial\Omega_{2-in}} = Q_{\partial\Omega_3}$	$12.7[kW]$
$Q_{\partial\Omega_{2-in}} = -Q_{\partial\Omega_1}$	$12.7[kW]$
T_{Sat}	From experiments (see **Figure 2**)

4. Results and discussion

The condensing behavior and evaporating dynamics of refrigerant R404a have been simulated using the VOF approach. Due to the temperature difference, and heat flux, the refrigerant condenses throughout the spiral tubing array, whereas sporadic evaporation occurs given the inertial and body forces present in the flow. The simulation was initialized by filling the total volume of the condenser section with both, the primary fluid (liquid water) and the secondary fluid domain (refrigerant) in a vapor state.

Figure 4 shows the domain initialization at t = 0.0 s. After this instant, the water starts to flow while the refrigerant is still in a full vapor state. The magnitude and direction of the water velocity is presented by the streak line in the internal flow section, and the quality of the secondary flow is indicated by the contour interface.

At t = 0.15 s, the refrigerant leaving the condenser has fully condensed near the outlet section based on the sub-cooled temperature boundary condition. Upstream the copper tube, the refrigerant begins a phase-transitioning throughout the lower section of the spiral geometry (shown in **Figure 5**) induced by the fluid temperature distribution.

The two-phase flow in the copper tube shows complicated details, with various phase-transition patterns and irregular oscillation manifesting at the periphery of the geometry due to the centrifugal [42] and inertial forces. The mean vapor quality found in the refrigerant region is 60%.

The water around the copper elbow carrying vapor refrigerant near the inlet develops a high velocity zone due to the reduction of area enhancing the heat flux in

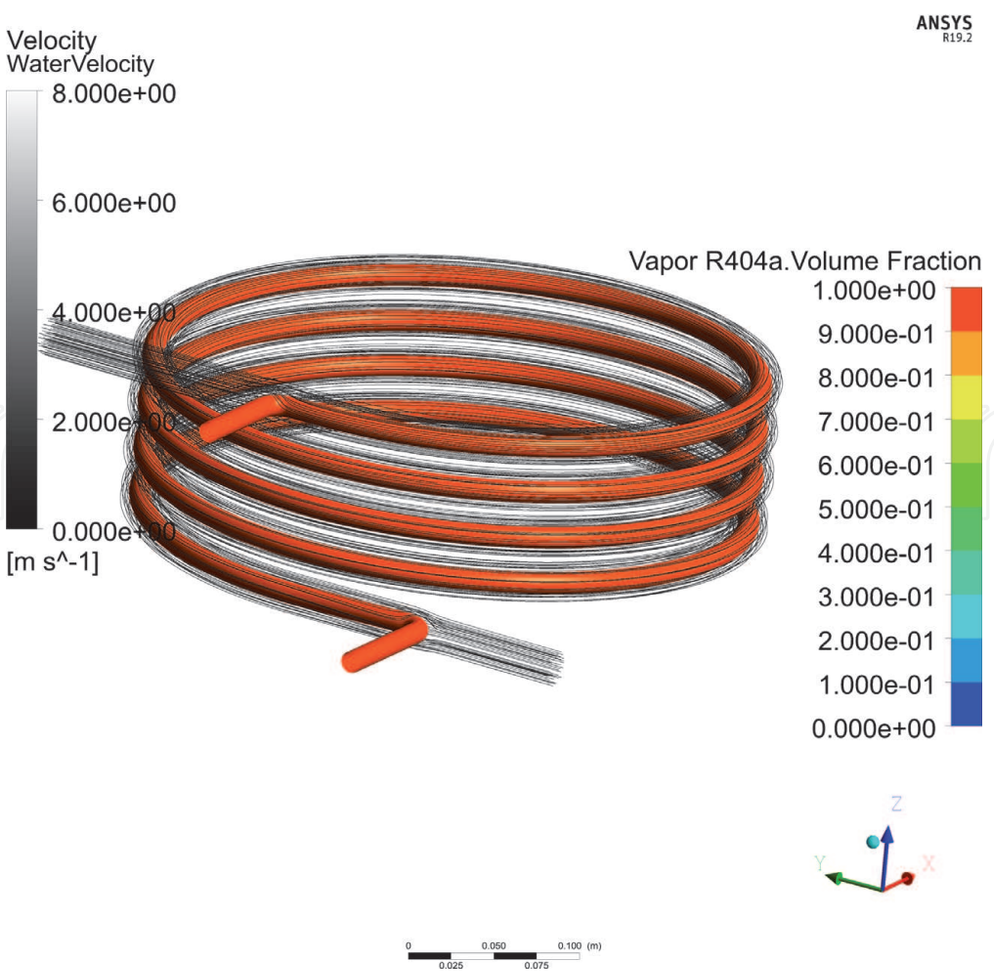

Figure 4.
Numerical solution of the phase transition of R404a in the water-condenser at t = 0.0 s.

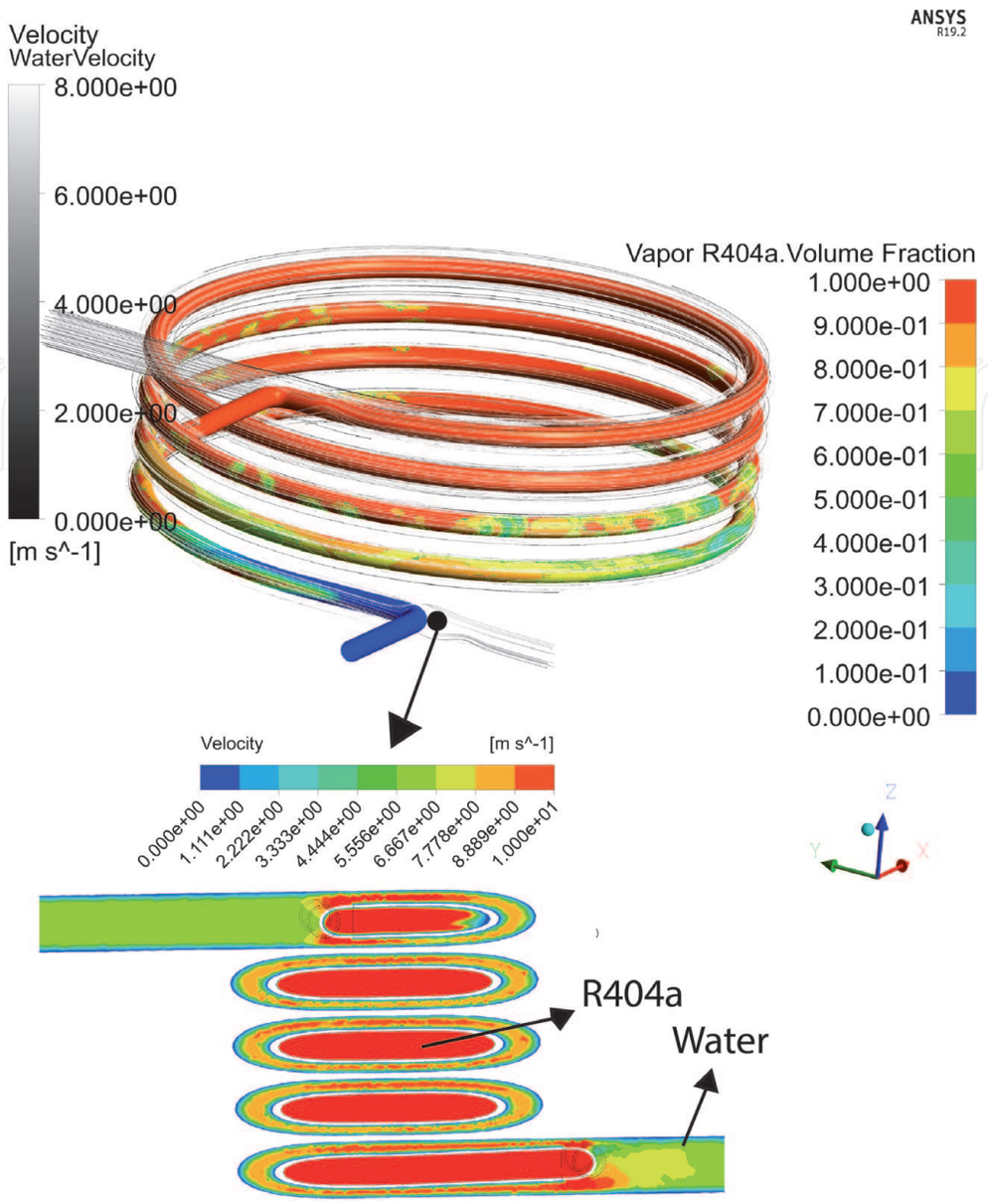

Figure 5.
Phase-transition and velocity field development at the outlet of the condenser at t = 0.15 s.

the system [43]. On the other hand, the vapor refrigerant develops a vortex pair at the beginning of the first spiral. This is probably induced by the tube curvature close to the inlet elbow. Interestingly, no other vortices develop in subsequent curved regions which suggests that the vortex develops due to the thermal and inertial characteristics of the vapor refrigerant entering the tubular array and the proximity to the 90° elbow located at the inlet.

Figure 6 shows the refrigerant phase transition details at 0.5 s. At this instant, the refrigerant has completely transitioned to liquid at the last quarter of the spiral leading to the outlet of the condenser. In the middle section of the condenser, the saturated vapor condenses and evaporates along the outer wall in repeated patters of saturated vapor and multi-phase flow swirling due to gravity and rotational speed.

Since the wall temperature across the copper wall was assumed constant, the phase-transition region extends across a large region of the tubular array. This boundary condition prevented a flash point transition between phases [44]. Furthermore, the outlet temperature was specified to remain in a sub-cool state allowing the saturated liquid to develop further into the inner regions of the condenser.

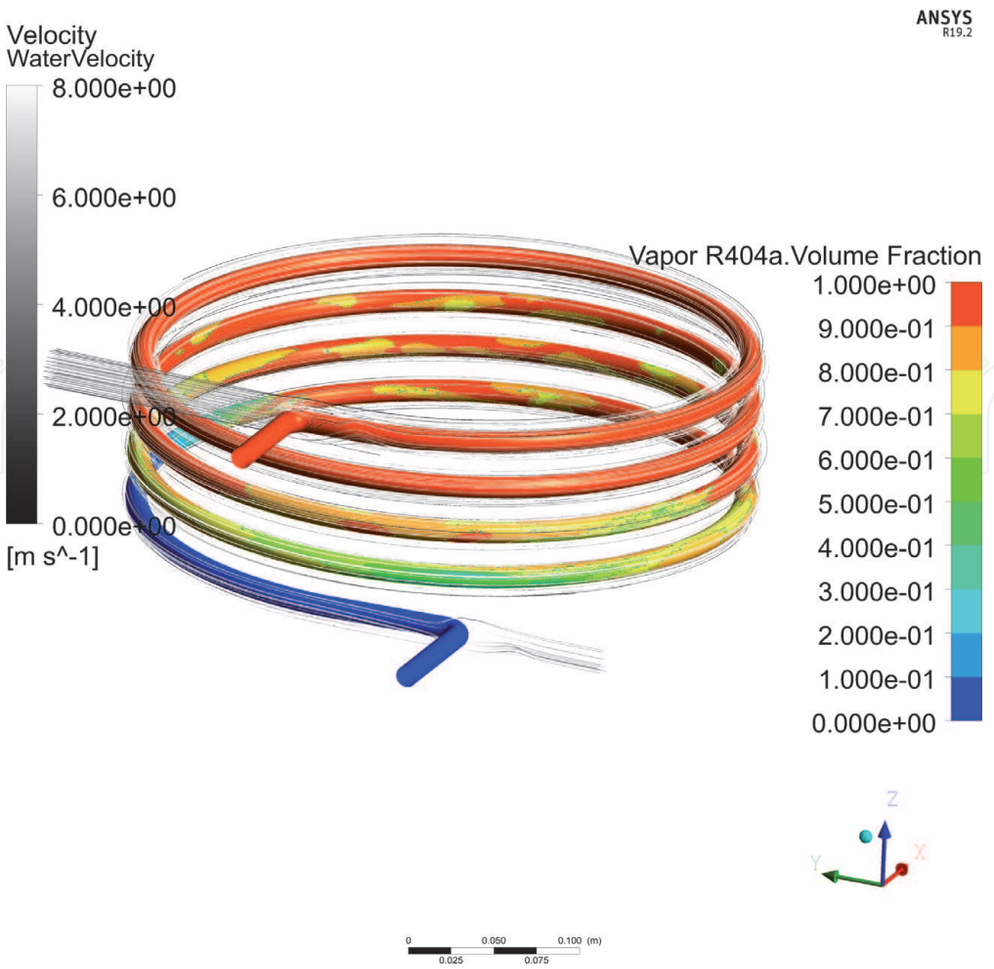

Figure 6.
Numerical solution of the phase transition of R404a in the water-condenser at t = 0.5 s.

Figure 7 shows the condensing and evaporating characteristics of R404a at t = 1.25 s. At the tube periphery and after the first revolution, the saturated vapor begins to condense, transitioning into a two-phase flow with a 90% quality and further decreasing into a quality of 82% while displaying a parabolic profile along the outer surface wall. Then, the mixture evaporates back to a saturated vapor state before it reaches its full condensation state after the third revolution.

Since the heat transfer can be enhanced or penalized by geometrical factors [45], the widely used Dittus-Boelter (Eq. (17)) was employed to find the Nusselt number in the internal tubing section for the vapor refrigerant flow. Based on the fundamental restrictions of the geometry, parametric modifications to the equation determining the Nusselt number (Eq. (18)) need to be considered based on constant wall temperature assumptions [46], curvature ration [47], and fluid regime [48] such that:

$$Nu_v = \frac{\left(\frac{f}{8}\right) Re_v Pr_v}{1.07 + 12.7\left(\frac{f}{8}\right)^{0.5}\left(Pr_v^{0.66} - 1\right)} \quad 4e3 < Re < 5e6, 0.5 < Pr < 2e3 \tag{17}$$

and

$$Nu_{v-HLX} = Nu_v\left(1 + 0.35\left(\frac{D_{\Omega_{3-\infty}}}{D_{\mathrm{HLx}}}\right)\right). \tag{18}$$

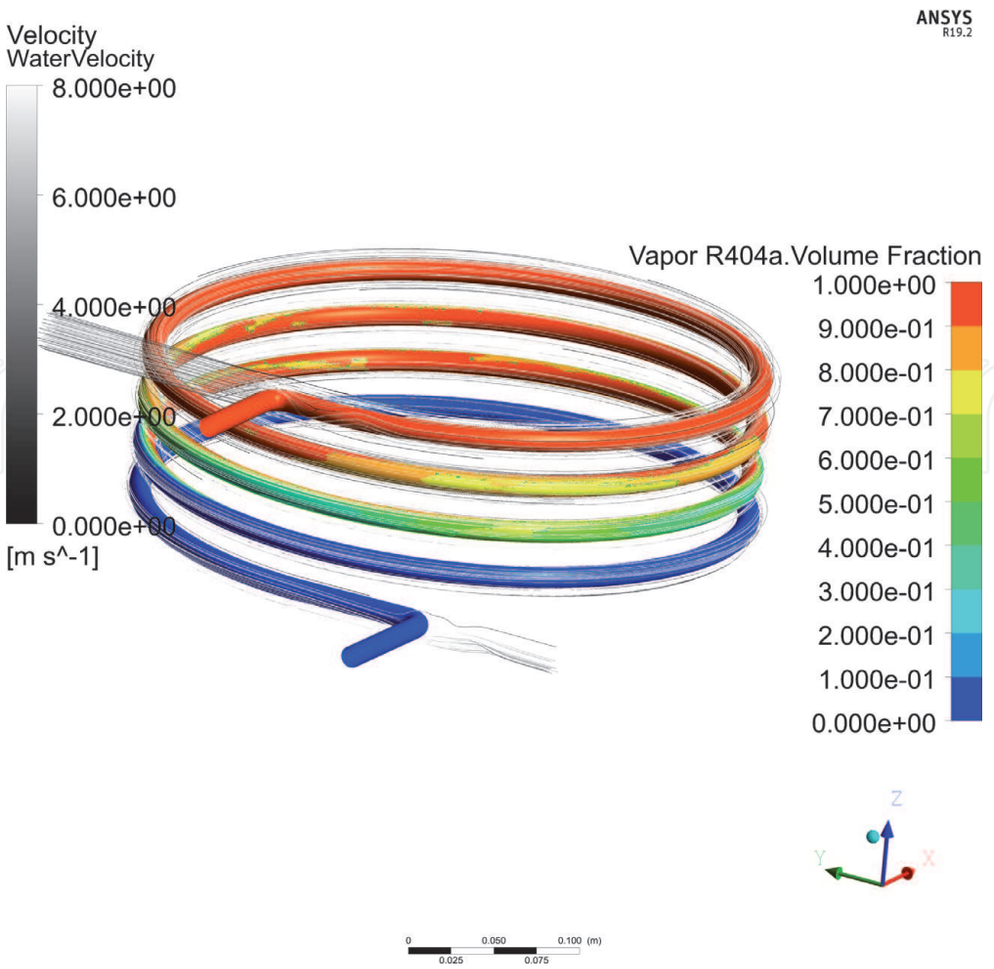

Figure 7.
Numerical solution of the phase transition of R404a in the water-condenser at t = 1.25 s.

where the friction factor is given by:

$$f = (1.82 \ln Re - 1.62)^{-2} \tag{19}$$

given that the Prandtl and Reynolds numbers are:

$$Pr_v = \frac{\mu_v c_{p-v}}{K_v} \tag{20}$$

and

$$Re = \frac{\rho_v \vec{u}_v D_{\Omega_3}}{\mu_v}. \tag{21}$$

Figure 8 shows the Nusselt number with respect to vapor refrigerant mass flow as a function different tube diameter. For $D_{\Omega_3} = 0.0063m$, the Nusselt number calculated ranges between 900 and 1500 at different vapor mass flows. On the other hand, the Nusselt number at $D_{\Omega_3} = 0.0191m$, ranges between 2250 and 4200, suggesting that the heat transfer enhancement occurs by increasing the diameter of the refrigerant line and reducing the number of spirals.

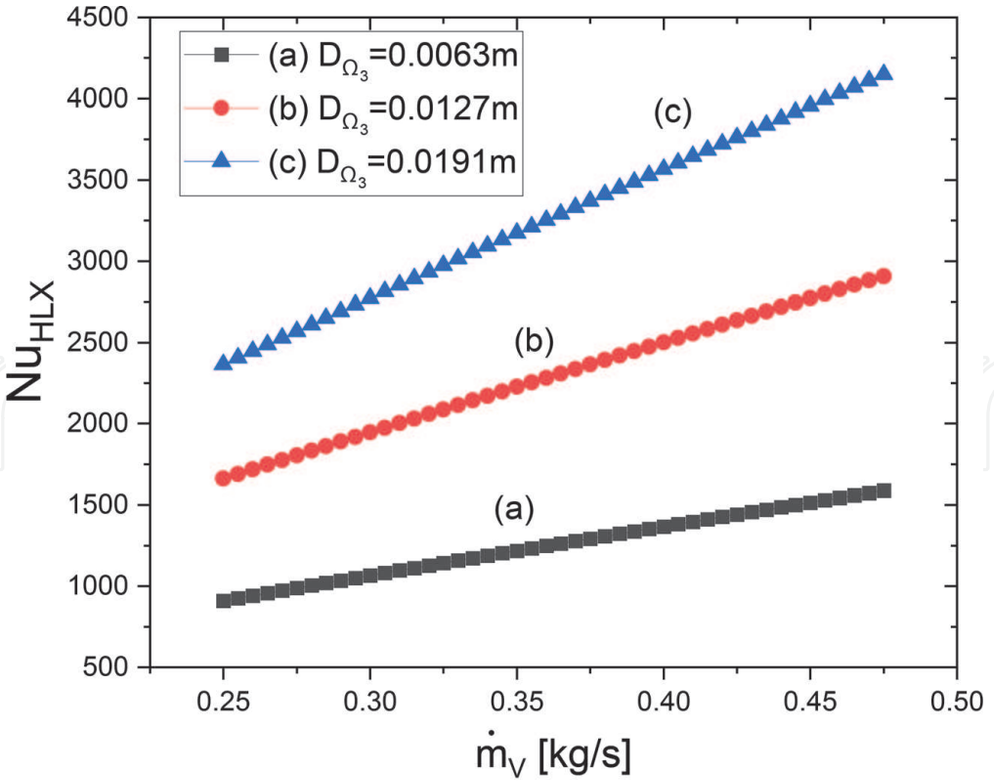

Figure 8.
Predicted Nusselt number as a function vapor refrigerant mass flow as a function of inlet diameter.

5. Conclusions

A time and temperature dependent three-dimensional multi-phase simulation with dynamics boundary conditions determined experimentally has been developed to characterize the thermal, inertial, and phase-transition details of refrigerant R404a in a water-cooled condenser at startup conditions. Given the complicated geometrical configuration of the system, where the secondary fluid (refrigerant) is concentric and flows inside the copper jacket in contact with the primary fluid (water), it becomes a challenging task to capture experimental information about the phase-transition details of the refrigerant using common optical or fluid field experimental methods such as optical tagging, particle image velocimetry, or tomography techniques. Therefore, indirect methods have been applied to obtain temperature and pressure values at the inlet and outlet sections of the condenser.

The numerical solution showed the condensing and evaporating oscillatory nature of the phase-transition throughout the spiral tubbing as well as the progression of saturated liquid at the outlet of the refrigerant line. Condensation occurs due to the temperature differences between the water and the refrigerant. Evaporation takes place given the body and inertial forces present in the system that prevent further bubble nucleation to sustain the condensation process.

The velocity profiles for both water and refrigerant show vortices developing at the inlet and outlet zones due to the curvatures and elbows present in the geometry. Nusselt numbers show that heat transfer can be optimized by slightly increasing the diameter of the refrigeration line without inducing a disruption in the flow regime or affecting the manufacturability of the part.

Acknowledgements

The author is grateful to FBD L.P. for the financial support to perform the experimental analysis.

Conflict of interest

The author declares no conflict of interest.

Nomenclature

A_s	Surface area $[m^2]$
D	Diameter$[m]$
h	Enthalpy $\left[\frac{kJ}{kg}\right]$
S	Source
T	temperature $[K]$
t	Time $[s]$
V	Volume
$\overrightarrow{u}$	Velocity $\left[\frac{m}{s}\right]$
x	Quality

Subscripts

cr	Critical
cu	Copper
eff	Effective
l	Liquid
o	Reference
Ref	Refrigerant
sat	Saturation
v	Vapor

Greek letters

α	Vapor volume fraction
ρ	Density
ξ	Surface tension $\left[\frac{N}{m}\right]$
ς	Mass transfer intensity $\left[\frac{1}{s}\right]$
$\overline{\overline{\tau}}$	Stress tensor $[Pa]$
μ	Viscosity
Ω	$3D$ domain

Author details

Carlos Acosta
The University of Texas at San Antonio, San Antonio, Texas

*Address all correspondence to: carlos.acosta2@utsa.edu

References

[1] J. Bustamante, A. Rattner and S. Garimella, "Achieving near-water-cooled power plant performance with air-cooled condensers," Applied Thermal Energy, vol. 105, pp. 362–371, 2016.

[2] G. Heidinger, S. Nascimento, P. Gaspar and P. Silva, "Experimental evaluation of the thermal performance at different environmental conditions of a low temperature display case with built-in compressor and water-cooled condenser," Applied Thermal Engineering, vol. 144, pp. 825–835, 2018.

[3] T. Veldkamp, Y. Wada, J. Aerts, P. Doll, S. Gosling, L. Ja, Y. Masaki, T. Oki, S. Ostberg, Y. Pokhrel, Y. Satoh, H. Kim and P. Ward, "Water scarcity hotspots travel downstream due to human interventions in the 20th and 21st century," Nat Commun, vol. 8, pp. 1–12, 2017.

[4] C. Aprea, R. Mastrullo and C. Renno, "Experimental analysis of the scroll compressor performances varying its speed," Applied Thermal Engineering, vol. 26, no. 10, pp. 983–992, 2006.

[5] P. Donnellan, K. Cronin and E. Byrne, "Recycling waste heat energy using vapour absorption heat transformers: A review," Renew. Sustain. Energy Rev, vol. 42, pp. 1290–1304, 2015.

[6] A. Babiloni, J. Esbrí, C. Cervera, F. Molés and B. Peris, "Analysis based on EU Regulation No 517/2014 of new HFC/HFO mixtures as alternatives of high GWP refrigerants in refrigeration and HVAC systems," International Journal of Refrigeration, vol. 52, pp. 21–31, 2015.

[7] "System Drop-in Testing of R-410A Replacements in Split System Heat Pump," *Air-Conditioning, Heating, and Refrigeration Institute (AHRI) Low-GWP Alternative Refrigerants Evaluation Program (Low-GWP AREP)*, vol. Test report #22., 2013.

[8] C. Acosta, D. Yanes, A. Bhalla, R. Guo, E. Finol and J. Frank, "Numerical and experimental study of the glass-transition temperature of a non-Newtonian fluid in a dynamic scraped surface heat exchanger," International Journal of Heat and Mass Transfer, vol. 152, pp. 1–8, 2020.

[9] C. Acosta, A. Bhalla and R. Guo, "Empirical and numerical determination of the freezing point depression of an unsteady flow in a scraped surface crystallizer," Applied Thermal Engineering, vol. 179, pp. 1–8, 2020.

[10] Y. Shang, . Y. Zhang, . Y. Hou, B. Bai and X. Zhong, "Effects of surface subcooling on the spreading dynamics of an impact water droplet," Physics of Fluids, vol. 32, pp. 1–10, 2020.

[11] S. Richter, S. Fleischer, M. Aritomi and R. Hamp, "Transient two-phase flow in arbitrary inclined tubes caused by depressurization of liquid with dissolved gasses," International Journal of Heat and Mass Transfer, vol. 44, no. 1, pp. 1–15, 2001.

[12] R. Akasaka, "Thermodynamic property models for the difluoromethane (R-32) + trans-1,3,3,3-tetrafluoropropene (R-1234ze(E)) and difluoromethane + 2,3,3,3-tetrafluoropropene (R-1234yf) mixtures," Fluid Phase Equilibria, vol. 358, pp. 98–104, 2013.

[13] D. Frenkel and B. Smit, Understanding molecular simulation: from algorithms to applications, San Diego: Academic Press, 2001.

[14] T. He, C. Mei and J. Longtin, "Thermosyphon-assisted cooling system for refrigeration applications," International Journal of Refrigeration, vol. 74, pp. 165–176, 2017.

[15] J. Kim, C. Han and S. Jeong, "Disturbance observer-based robust control against model uncertainty and

disturbance for a variable speed refrigeration system," International Journal of Refrigeration, vol. 116, pp. 49–58, 2020.

[16] C. Truesdell, The Tragicomedy of Classical Thermodynamics, Vienna: 1971, Springer.

[17] Z. Wu and R. Du, "Design and experimental study of a miniature vapor compression refrigeration system for electronics cooling," Applied Thermal Engineering, vol. 31, no. 2, pp. 385–390, 2011.

[18] S. Mimouni, A. Foissac and J. Lavieville, "CFD modelling of wall steam condensation by a two-phase flow approach," Nuclear Engineering and Design, vol. 241, no. 11, pp. 4445–4455, 2011.

[19] D. Sun, J. Xu and Q. Chen,, "Modeling of the evaporation and condensation phasechange problems with FLUENT," Heat Transf., Part B: Fundamentals, vol. 66, no. 4, pp. 326–342, 2014.

[20] S. Mimouni, "CFD modeling of wall steam condensation: two-phase flow approach versus homogeneous flow approach," *Sci. Technol. Nucl. Install,* 2011.

[21] H. Mohammed, D. Giddings and G. Walker, "CFD multiphase modelling of the acetone condensation and evaporation process in a horizontal circular tube," International Journal of Heat and Mass Transfer, vol. 134, pp. 1159–1170, 2019.

[22] N. Padoin and C. Soares,, "CFD modeling of steam condensation in industrial pipes,," Blucher Chem. Eng. Proc, vol. 1, no. 2, p. 12904–12911, 2015.

[23] M. Konopacki, M. Kordas, K. Fijalkowski and R. Rakocz, "Computational fluid dynamics and experimental studies of a new mixing element in a static mixer as a heat exchanger," Chem. Process Eng, vol. 36, no. 1, pp. 59–72, 2015.

[24] G. Anjos, G. Oliveira and M. Norberto, "Arbitrary Lagrangian–Eulerian Method for Two-Phase Flows: Applications," in *Encyclopedia of Two-Phase Heat Transfer and Flow III*, World Scientific, 2018, pp. 141–183.

[25] J. Parekh and R. Rzehak, "Euler–Euler multiphase CFD-simulation with full Reynolds stress model and anisotropic bubble-induced turbulence," International Journal of Multiphase Flow, vol. 99, pp. 231–245, 2018.

[26] M. Göz, S. Lain and M. Sommerfeld, "Study of the numerical instabilities in Lagrangian tracking of bubbles and particles in two-phase flow," Comput. Chem. Eng, vol. 28, p. 2727–2733, 2004.

[27] E. E. Michaelides, "Review—The Transient Equation of Motion for Particles, Bubbles, and Droplets," J. Fluids Eng., vol. 119, no. 2, pp. 1–16, 1997.

[28] H. Hu, "Direct simulation of flows of solid-liquid mixtures," International Journal of Multiphase Flow, vol. 22, no. 2, pp. 335–352, 1996.

[29] A. Arora and S. Kaushik, "Theoretical analysis of a vapour compression refrigeration system with R502, R404A and R507A," International Journal of Refrigeration, vol. 31, no. 6, pp. 998–1005, 2008.

[30] M. Zareh, H. Shokouhmand, M. Salimpour and M. Taeibi, "Numerical simulation and experimental analysis of refrigerants flow through adiabatic helical capillary tube," International Journal of Refrigeration, vol. 38, pp. 299–309, 2014.

[31] S. Lee, M. Kim and S. Ro, "Thermal Conductivity of 1,1,1-Trifluoroethane (R143a) and R404A in the Liquid Phase," Journal of Chemical and Engineering Data, vol. 46, no. 5, pp. 1013–1015, 2011.

[32] "Pure and Pseudo-pure Fluid Thermophysical Property Evaluation

and the Open-Source Thermophysical Property Library CoolProp," *Industrial and Engineering Chemistry Research,* vol. 53, no. 6, pp. 2498–2508, 2014.

[33] D. Green and R. Perry, Perry's Chemical Engineers' Handbook, London: McGraw-Hill, 2007.

[34] B. Fadhl, L. Wrobel and H. Jouhara, "CFD modelling of a two-phase closed thermosyphon charged with R134a and R404a," Applied Thermal Engineering, vol. 78, no. 5, pp. 482–490, 2015.

[35] W. Callister and D. Rethwisch, Materials sicnce and engineering an introduction, Wiley, 2010.

[36] V. Geller, D. Bivens and A. Yokozeki, "Viscosity of Mixed Refrigerants, R404A, R407C, R410A, and R507C," in *Int. Ref. and Air cond.*, West lafayette, 2000.

[37] E. Lemmon, M. Huber and M. McLinden, NIST standard reference database 23: reference fluid thermodynamic and transport properties-REFPROP, version 8.0, Gaithersburg: Standard Reference Data, 2007.

[38] A. Gadelha, S. Neto, R. Swarnakar and A. Lima, "Thermo-Hydrodynamics of Core-Annular Flow of Water, Heavy Oil and Air Using CFX," Advances in Chemical Engineering and Science, vol. 3, no. 4A, pp. 37–45, 2013.

[39] R. Heide, "The surface tension of HFC refrigerants and mixtures," *nt J.* Refrig, vol. 20, pp. 496–503, 1997.

[40] W. Lee, A pressure iteration scheme for two-phase flow modeling. Multiphase Transport Fundamentals, Reactor Safety, Applications, Washington, DC: Hemisphere Publishing, 1980.

[41] C. Acosta, A. Bhalla and R. Guo, "Phase-transition temperature determination using optical spectroscopy in a rotating flow inside a scrape surface crystallizer," in *Photonic Fiber and Crystal Devices: Advances in Materials and Innovations in Device Applications XIV*, San Diego, 2020.

[42] H. Wu, X. Peng, P. Ye and Y. Gong, "Simulation of refrigerant flow boiling in serpentine tubes," Transfer, International Journal of Heat and Mass, vol. 50, no. 5, pp. 1186–1195, 2007.

[43] H. Ito, "Flow in Curved Pipes," JSME international journal, vol. 30, pp. 543–551, 1987.

[44] A. Seixlack and M. Barbazelli, "Numerical analysis of refrigerant flow along non-adiabatic capillary tubes using a two-fluid model," Applied Thermal Engineering, vol. 29, no. 2, pp. 523–531, 2009.

[45] J. Abraham, E. Sparrow and W. Minkowycz, "Internal-flow Nusselt numbers for the low-Reynolds-number end of the laminar-to-turbulent transition regime," International Journal of Heat and Mass Transfer, vol. 54, no. 1, pp. 584–588, 2011.

[46] R. Seban and E. McLaughlin, "Heat transfer in tube coils with laminar and turbulent flow," International Journal of Heat and Mass Transfer, vol. 6, no. 5, pp. 387–395, 1963.

[47] H. Zhao, X. Li, Y. Wu and X. Wu, "Friction factor and Nusselt number correlations for forced convection in helical tubes," International Journal of Heat and Mass Transfer, vol. 155, p. 119759, 2020.

[48] L. Janssen and C. Hoogendoorn, "Laminar convective heat transfer in helical coiled tubes," International Journal of Heat and Mass Transfer, vol. 21, no. 9, pp. 1197–1206, 1978.